www.acsami.org Research Article

Selective Pulsed Chemical Vapor Deposition of Water-Free TiO_2/Al_2O_3 and HfO_2/Al_2O_3 Nanolaminates on Si and SiO_2 in Preference to SiCOH

James Huang, Yunil Cho, Zichen Zhang, Antony Jan, Keith T. Wong, Srinivas D. Nemani, Ellie Yieh, and Andrew C. Kummel*

Cite This: ACS Appl. Mater. Interfaces 2022, 14, 15716−15727 Read Online

ACCESS | Metrics & More | Article Recommendations | Supporting Information

ABSTRACT: Highly selective and smooth TiO_2/Al_2O_3 and HfO_2/Al_2O_3 nanolaminates were deposited by water-free pulsed chemical vapor deposition (CVD) at 300 °C using titanium isopropoxide ($Ti(O^iPr)_4$) and hafnium tertbutoxide ($Hf(O^tBu)_4$) with trimethylaluminum (TMA). TMA was found to be the key factor for enhancing nucleation selectivity on SiO_2 or Si versus SiCOH (hydrophobic, nonporous low *k* dielectric). With precise dosing of TMA, selective nucleation of TiO_2/Al_2O_3 and HfO_2/Al_2O_3 nanolaminates was achieved and smoother films were formed with higher selectivity compared to single precursor TiO_2 and HfO_2 CVD. The selectivity of TiO_2/Al_2O_3 nanolaminate deposition increased from 34 to 44 (deposition on Si vs SiCOH), while RMS roughness of the film of Si decreased from 2.8 to 0.38 nm. The selectivity of HfO_2/Al_2O_3 deposition increased from 14 to 73, while the RMS roughness of HfO_2/Al_2O_3 on Si was maintained at a similar value of 0.78 nm. Deposition of water-free pulsed CVD TiO_2/Al_2O_3 and HfO_2/Al_2O_3 nanolaminates was conducted on a Cu/SiCOH patterned sample to study their nanoselectivity. Transmission electron microscopy images of the Cu/SiCOH patterned sample demonstrated that highly selective and smooth TiO_2/Al_2O_3 and HfO_2/Al_2O_3 nanolaminates can be formed on a nanoscale pattern.

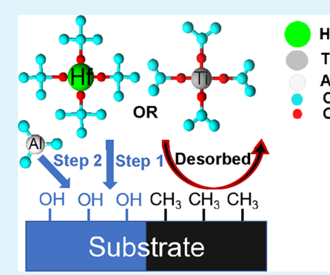

KEYWORDS: *water-free oxide deposition, area-selective pulsed chemical vapor deposition, titanium isopropoxide, hafnium tertbutoxide, nanolaminate*

Downloaded via UNIV OF CALIFORNIA SAN DIEGO on May 20, 2022 at 05:48:29 (UTC).
See https://pubs.acs.org/sharingguidelines for options on how to legitimately share published articles.

■ INTRODUCTION

Ultraviolet (UV) photolithography technology is one of the key components in the semiconductor industry. Advancement in the transistor density of integrated circuits (ICs) can be partially attributed to the improvement in the UV photolithography process.[1,2] When scaling down the size of a metal oxide semiconductor field effect transistor (MOSFET), mask misalignment became one of the major limitations of UV photolithography.[3−6] To solve the issue of mask misalignment, Bencher et al. proposed the self-aligned chemical vapor deposition (CVD) [or area-selective CVD (AS-CVD)] spacer double-patterning method which has evolved to a self-aligned quadruple-patterning method in recent years.[7,8] The spacer or etch stop material when selectively deposited onto the preferred locations of a pre-etched structure allows the pitch of the IC to be reduced by half. Since then, AS-CVD has garnered attention as an alternative patterning method.

Previously, TiO_2 HfO_2, and Al_2O_3 were demonstrated to be possible spacers or etch stop layers in self-aligned patterning.[9] HfO_2 and Al_2O_3 can also act as diffusion barriers for Cu interconnects as demonstrated by Majumder et al.[10] In a recent study by Chen et al., TiO_2 is reported to be a strong candidate for dielectric-on-dielectric CVD to achieve self-aligned via integration with alkanethiol self-assembly monolayers (SAMs) for selective deposition.[11]

CVD process normally involves one or more gas-phase precursors reacting near the substrate surface.[12] For thermal CVD, the focus of the present study, gas-phase precursors physisorb onto the substrate surface and potentially chemisorb with a reactive site such as a hydroxyl group (OH^-). Due to the high surface temperature, the chemisorbed precursors will undergo decomposition and may form new reactive (OH^-) sites. This leads to continuous deposition without a self-limiting step, but pulsed CVD can result in self-limiting adsorption since the physisorption process can be limited to a single monolayer.

AS-CVD can be achieved by three methods: inherent selectivity, selective passivation, and selective activation.[13−15] Inherent selectivity is the most desired since it is economically feasible and undemanding; in this process, selectivity is

Received: October 13, 2021
Accepted: March 10, 2022
Published: March 22, 2022

achieved by the difference in reactivity between two substrate surfaces. Conversely, selective passivation and selective activation require one extra step of passivant (or activant) deposition.

In the present study, inherently, AS-CVD was achieved by utilizing the difference in surface reactivity (e.g., the number of Si−OH or Si−H sites) between Si, SiO_2, and alkyl (CH_3^-) terminated Si (SiCOH). Selectivity was defined by the following equation and evaluated when the film thickness on SiCOH approached 0.3 nm, which is less than 1 monolayer[16] (a more common selectivity metric is provided in the Supporting Information S1)

$$\text{selectivity} = \frac{\text{film thickness on Si}}{\text{film thickness on SiCOH}}$$

In our earlier works, selective water-free single precursor TiO_2 and HfO_2 pulsed CVD deposition on Si, SiO_2, and SiCOH was studied.[17,18] SiCOH is an unreactive surface but requires a water-free process to avoid hydroxylation which can result in both loss of selectivity and substrate oxidation.

At 300 °C, water-free TiO_2 pulsed CVD was achieved by pulsed dosing of titanium isopropoxide [$Ti(O^iPr)_4$] precursor instead of continuous flow. HfO_2 water-free pulsed CVD at 300 °C has been studied by Cho et al. using hafnium *tert*-butoxide [$Hf(O^tBu)_4$] as the single precursor. When pulsed gas-phase $Ti(O^iPr)_4$ precursor adsorbs onto the substrate surface, it decomposes into TiO/TiOH and OiPr/iPr ligand. TiO/TiOH will chemisorb onto the substrate (OH^-) and (H^+) sites, while remaining ligands will be removed during the nitrogen gas purging 1/2 cycle. Sequential pulses of $Ti(O^iPr)_4$ are expected to follow the same mechanism and form TiO_2 layers. The use of multiple short pulses instead of longer pulses affords the ligands time to desorb and the physisorbed precursor on nonreactive surfaces time to desorb.

Optimization of the pulsed single precursor CVD process (substrate time and pulse lengths) increases selectivity and prevents gas-phase reaction and uncontrollable growth rate.[18] Around 17 and 40 nm TiO_2 were selectively deposited on Si and SiO_2 in preference to SiCOH (≤0.5 nm) with a selectivity of 34 on the Si surface.[17] Pulsed water-free $Hf(O^tBu)_4$ CVD proceeds by a similar mechanism and deposited 1.8 and 5 nm of HfO_2 on Si and SiO_2 in preference to SiCOH (0.13 nm) with a selectivity of 14 on Si versus SiCOH.[18] Note, the selectivity was greater for SiO_2 versus Si but was quantified for Si versus SiCOH since the thickness was more accurately measured by ellipsometry on Si. However, despite the superior selectivity, the deposited TiO_2 films showed high surface roughness due to crystallization (shown in Figure S3). This is nonideal for high-density MOSFET devices.

A TiO_2/Al_2O_3 nanolaminate structure on Si was previously demonstrated by Testoni et al. to be free of nanocrystallites because Al_2O_3 cannot crystallize at normal atomic layer deposition (ALD) or CVD temperatures, and crystallization is impeded for TiO_2.[19] This nanolaminate structure was accomplished by employing ALD supercycles of $Ti(O^iPr)_4$ with H_2O and trimethyl aluminum (TMA) with H_2O.[19] Later, Ylivaara et al. studied the growth and mechanical properties of TiO_2/Al_2O_3 nanolaminate ALD using $TiCl_4$ and TMA with H_2O as the coreactant.[20] Yang et al. showed that the HfO_2/Al_2O_3 nanolaminate had better electrical properties than just pure HfO_2 or Al_2O_3.[21]

Even though there have been many studies about the electrical, mechanical, and even optical properties of TiO_2, HfO_2, and their nanolaminates with Al_2O_3, little is known about the water-free TiO_2/Al_2O_3 and HfO_2/Al_2O_3 nanolaminates pulsed AS-CVD processes and their selectivity performance.[22−27] Our group previously reported the selectivity and surface smoothness of a water-free HfO_2/TiO_2 nanolaminate pulsed CVD.[28] The nanolaminate structure was found to be the key factor that can impede the formation of nanocrystallites if the sublayer is about 1.5 nm (a schematic nanolaminate illustration is shown in Figure 1).[28] However,

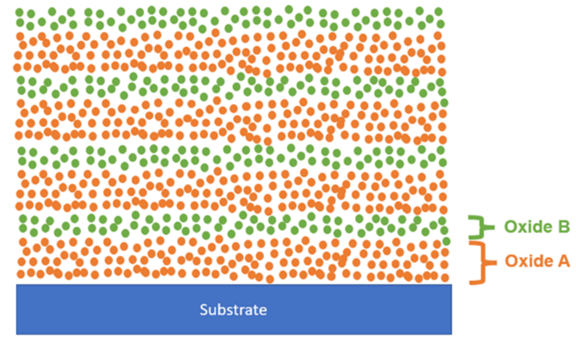

Figure 1. Schematic diagram showing a nanolaminate structure with alternating oxide A and oxide B sublayers.

there was a large selectivity difference between pure HfO_2 and pure TiO_2 pulsed CVD deposition which leads to a reduced (∼16 nm with highest TiO_2 ratio) selective HfO_2/TiO_2 nanolaminate deposition on Si in preference to SiCOH.[28]

TMA is a well-studied precursor used with an oxidant coreactant for Al_2O_3 CVD.[29] Al in TMA is a strong electron donor which favors bond formation with oxygen, a strong electron acceptor.[19,30] TMA can act as an oxygen [(OH^-) group] scavenger and is a possible solution to achieve both high selectivity and film smoothness.[31] In the present study, it is shown that TMA enhances the selectivity and film smoothness of both TiO_2 and HfO_2 water-free pulsed CVD in nanolaminate stacks. Experiments were carried out at 300 °C which is the optimized dosing temperature calibrated for HfO_2 and TiO_2 thermal CVD processes.[17,18] At 300 °C, both TiO_2/Al_2O_3 and HfO_2/Al_2O_3 nanolaminates were deposited by supercycles of $Ti(O^iPr)_4/Hf(O^tBu)_4$ with TMA subcycles. The sublayers are designed to be about 1 nm in thickness to prevent nanocrystallite formation in the HfO_2 or TiO_2 sublayers. The optimal supercycles consisted of 200 pulses $Ti(O^iPr)_4$ with 1 pulse of TMA and 12 pulses of $Hf(O^tBu)_4$ with 1 pulse of TMA. Compared with single precursor TiO_2 pulsed CVD, for TiO_2/Al_2O_3 nanolaminates, selectivity on hydrofluoric acid (HF) cleaned Si versus SiCOH increased from 34 to 44, while RMS roughness of the film decreased from 2.8 to 0.38 nm. For HfO_2/Al_2O_3 nanolaminates, the selectivity for Si versus SiCOH increased from 13.8 to 73, and the film roughness was 0.78 nm. With the above supercycle recipes, nanoselectivity was also demonstrated on a Cu/SiCOH patterned sample.

The novelty of this paper is that a nanolaminate structure is used not only to mitigate nanocrystallite formation but also to improve the selectivity with the help of TMA. TMA is not just used as a precursor in this research but an additive to enhance smoothness and selectivity. This opens up the possibility for future dielectric nanolaminate fabrication.

https://doi.org/10.1021/acsami.1c19810
ACS Appl. Mater. Interfaces 2022, 14, 15716−15727

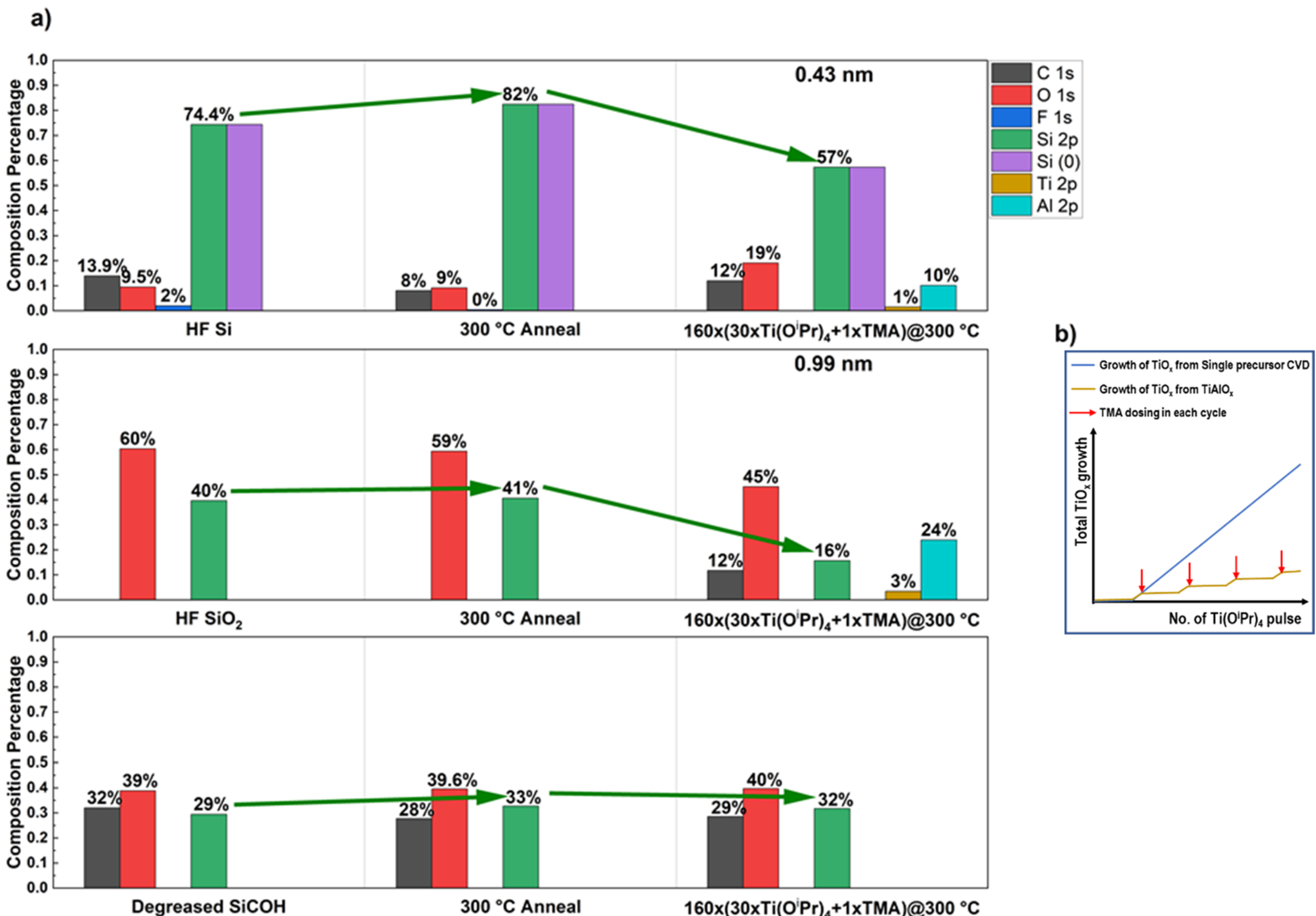

Figure 2. XPS study of nucleation for Ti/AlO$_x$ pulsed CVD. (a) XPS shows little to no growth of Ti/AlO$_x$ CVD with 30 pulses of Ti(O^{i}Pr)$_4$ followed by 1 pulse of TMA as a supercycle on HF-cleaned Si, SiO$_2$, and degreased SiCOH samples. XPS raw data can be found in Supporting Information Figure S4. (b) Heuristic model of the TiO$_2$ growth shows that TMA acts as a passivant in each supercycle suppressing the growth rate. Note these growth rates are just rough approximations for illustration.

EXPERIMENTAL SECTION

B-doped Si (0 0 1), SiO$_2$, SiCOH, and Cu/SiCOH-patterned samples were used as the substrate materials. All substrates underwent a degreasing process using acetone, methanol, and HPLC water sequentially for 10 s each. A N$_2$ air gun was used to remove residual aqueous solution on the substrate surface. For Si and SiO$_2$, after the degreasing process, an extra 30 s 0.5% HF clean followed by a HPLC water rinse was conducted. Afterward, the samples were loaded via a load lock into the deposition system.

SiCOH and Cu/SiCOH samples were obtained from Applied Materials (black diamond trade name). This SiCOH is a nonporous insulator. The SiCOH employed in the present study had 70 nm [80 nm before chemical mechanical polish (CMP)] thickness, a dielectric constant of 2.9, 20% carbon content, and ALD TaN with Co as the diffusion barrier material. The water contact angle for SiCOH was 82° before passivation and 88° after passivation (see below).

For the Cu/SiCOH samples received from Applied Materials, the pitch size was ~90 nm and the average linewidth was ~45 nm. Patterned SiCOH surface methyl groups can be damaged by plasma etching, UV lithrography, and even diffusion barrier sputtering processes which result in the formation of Si−H, Si−OH, and Si dangling bonds on the surface.[32−36] Similar to the silylation repair (forming a Si−O−CH_3 bond) demonstrated by Oszinda et al., passivation (damage repair) was performed using a proprietary process from Applied Materials to restore surface methyl concentration.[36] Degreased SiCOH samples were also passivated by this method as controls.

A custom-built vacuum chamber system was used for the CVD study (see chamber schematic diagram Figure S2). It consists of four vacuum chambers: load-lock chamber (for sample loading), CVD reaction chamber, and two ultra-high vacuum (UHV) chambers. Two or three samples (i.e., passivated Cu/SiCOH and passivated SiCOH or HF-cleaned Si, SiO$_2$, and degreased only SiCOH) were simultaneously loaded into the load-lock chamber. Therefore, a direct comparison of the nanolaminate CVD deposition thickness can be achieved for accurate selectivity measurements. A reaction chamber with a base pressure of 3×10^{-7} Torr was used for all experiments. This reaction chamber was pumped by a Pfeiffer TPU 062 turbo pump with backing by an Edwards RV3 rotary pump. There was a manipulator with a copper sample holder mounting platform inside the reaction chamber. A cartridge heater was inserted into this manipulator and used as a heat source during the CVD process. A N$_2$ purge line, TMA dosing line, Hf(O^{t}Bu)$_4$ dosing line, and Ti(O^{i}Pr)$_4$ dosing line were connected to the reaction chamber and pointed at the sample stage at a distance of 3 inches. Hf(O^{t}Bu)$_4$ (99.99%) and Ti(O^{i}Pr)$_4$ (99.99%) were both purchased from Sigma-Aldrich. TMA (98%) was purchased through Strem Chemicals.

Each dosing line contains at least one pneumatic ALD valve and a shut off valve. Hf(O^{t}Bu)$_4$ dosing line used two pneumatic valves to form a fixed volume to have better pressure control. For the N$_2$ purge line with a mass flow controller, an extra leak valve was installed to control its pressure. The reaction chamber wall and the dosing lines were wrapped with heat tape and kept at 150 °C. No push gas was employed for any of the precursors. Samples were preannealed to 300

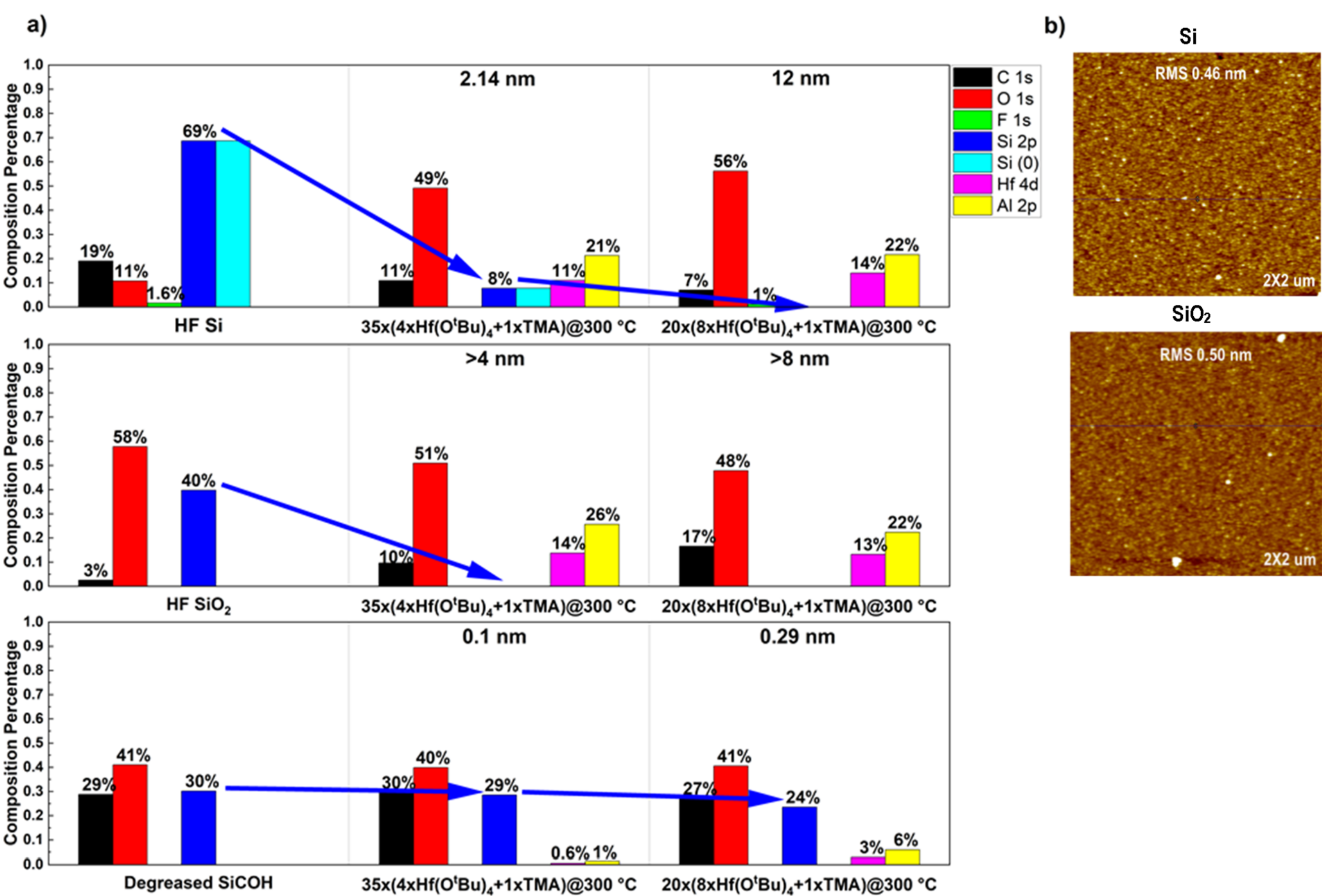

Figure 3. XPS study of nucleation for HF/AlO_x pulsed CVD. (a) XPS shows the growth suppression by TMA with 4 pulses of $Hf(O^tBu)_4$ in each supercycle, while 8 pulses of $Hf(O^tBu)_4$ per supercycle renders a higher selectivity than pure HfO_2 single precursor CVD. Raw data are shown in Supporting Information Figure S5. (b) Both AFM images on Si and SiO_2 samples show generally smooth film surfaces with RMS roughness of 0.46 and 0.50 nm, respectively.

°C in the UHV chamber before transferring to the ALD/CVD reaction chamber.

For the TiO_2/Al_2O_3 CVD reaction, the sample stage was heated to 300 °C. The $Ti(O^iPr)_4$ precursor bottle was kept at room temperature. For a supercycle, after a desired number of $Ti(O^iPr)_4$ pulses, 1 pulse of TMA was dosed. During the CVD process, continuous flow of N_2 purge gas was implemented. There were 60 s purge before and after each TMA pulse to prevent gas-phase reactions. In addition, continuous flow of N_2 purge gas was also implemented.

For the HfO_2/Al_2O_3 CVD reaction at 300 °C, the $Hf(O^tBu)_4$ precursor bottle was heated to 36 °C. The $Hf(O^tBu)_4$ source had two pneumatic valves to reduce the dose pressure. Both pneumatic valves have an opening time of 500 ms. After the first pneumatic valve opening, $Hf(O^tBu)_4$ gas flowed into a constant volume container; afterward, the first pneumatic valve was closed, and the gas was trapped for 10 s followed by the second pneumatic valve opening. Between each constant volume pulse, there is a 60 s N_2 purge in the reaction chamber. After the desired number of $Hf(O^tBu)_4$ pulses, there was a 60 s N_2 purge, a 15 ms TMA dose, and a 60 s N_2 purge. In addition, continuous flow of N_2 purge gas was also implemented.

After deposition, samples were transferred in vacuo to the UHV chamber where X-ray photoelectron spectroscopy (XPS) was performed. For XPS, a monochromatic Al Kα X-ray source (E = 1487 eV) and a hemispherical analyzer (XM 1000 MkII/SPHERA, Omicron Nanotechnology) with a pass energy of 50 eV were employed. The XPS anode voltage was set to 10 kV, and the filament emission current was set to 25 mA. For surface characterization, the XPS detector was aligned to 60° (glancing angle) from the sample surface normal. This angle was changed to 30° (normal angle) for bulk deposition compositional analysis. All XPS data were collected and analyzed by Casa XPS v2.3 program. Ex situ atomic force microscopy (AFM Agilent 5500) was employed to study the sample surface morphology. For cross-sectional studies of the samples focus ion beam and transmission electron microscopy (TEM) were performed.

■ RESULTS AND DISCUSSION

TMA as Reactive Site Scavenger and Selectivity Promoter. Water-free TiO_2/Al_2O_3 and HfO_2/Al_2O_3 pulsed CVD were performed on HF-cleaned Si, HF-cleaned SiO_2, and degreased SiCOH samples. HF-cleaned Si had its surface native oxide removed and had an Si−H terminated surface.[37] HF-cleaned SiO_2 and degreased SiCOH had Si−OH terminated and Si−CH_3 terminated surfaces, respectively.[18] From previous HfO_2/TiO_2 nanolaminate studies, thinner sublayers were known to prevent nanocrystallite formation.[28] A monolayer thickness of TiO_2 sublayer requires approximately 30 pulses of $Ti(O^iPr)_4$ (0.009 nm/pulse was calculated based on the single precursor TiO_2 pulsed CVD shown in Figure S3).[17] Consequently, the initial supercycle was composed of 30 pulses of $Ti(O^iPr)_4$ followed by 1 pulse of TMA 300 °C.

Figure 2a shows the XPS chemical composition of HF-cleaned Si, SiO_2, and degreased SiCOH as loaded, after 300 °C rapid anneal, and after the pulsed CVD deposition. Since all samples were preannealed to the CVD temperature before

https://doi.org/10.1021/acsami.1c19810
ACS Appl. Mater. Interfaces 2022, 14, 15716−15727

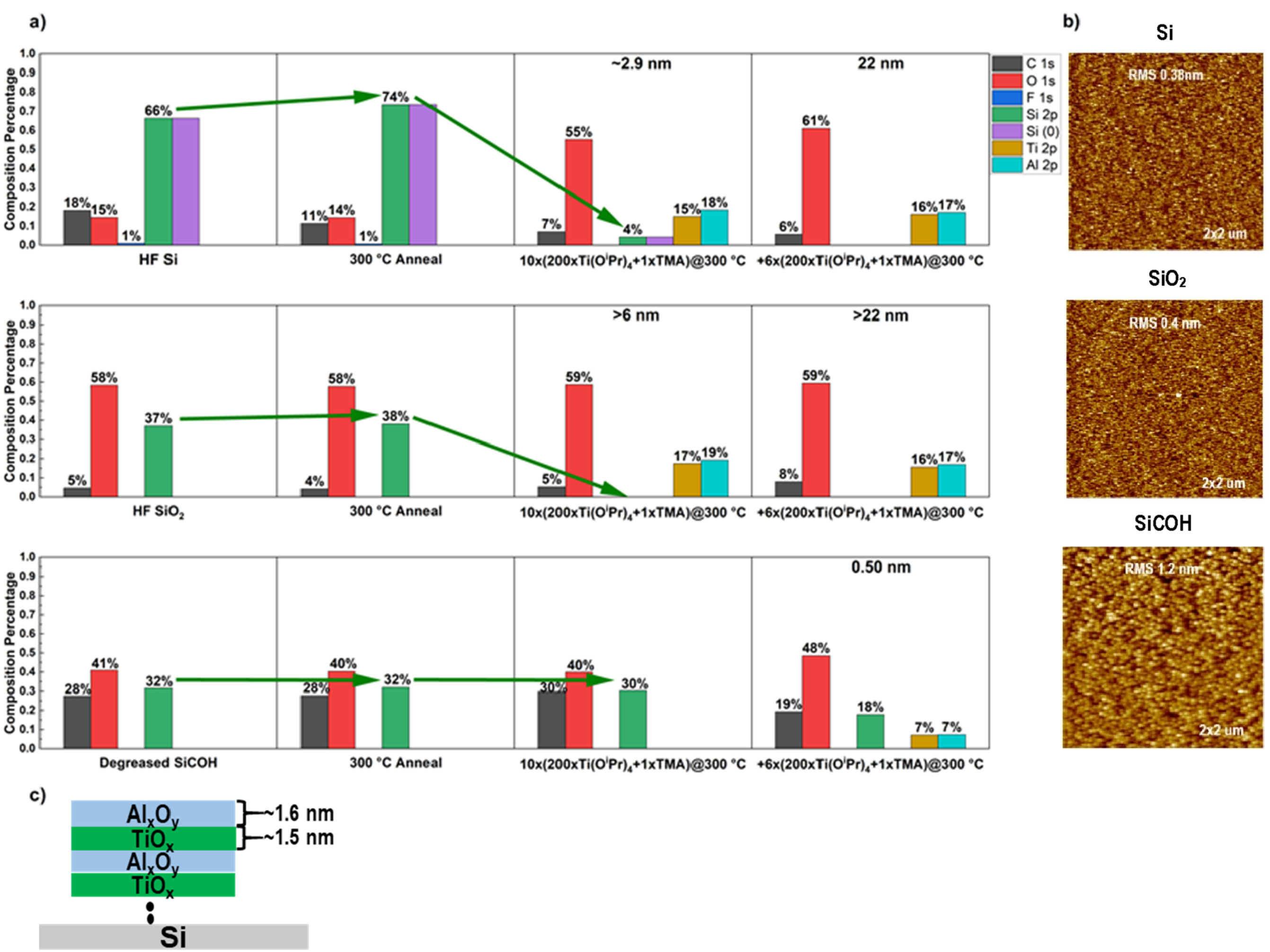

Figure 4. XPS study of selectivity for Ti/AlOx pulsed CVD. (a) $TiAlO_x$ CVD with single recipe (200 Ti pulses +1 TMA) XPS shows that around 22 nm of TiO_2/Al_2O_3 nanolaminate was selectively deposited on Si in preference to SiCOH. XPS raw spectra are shown in Figure S9. (b) AFM images show that both TiO_2/Al_2O_3 nanolaminate films are smooth on Si and SiO_2 with 0.38 and 0.40 nm RMS roughnesses, respectively. (c) Estimated nanolaminate structure composed of 1.6 nm of Al_2O_3 and 1.5 nm of TiO_2.

deposition, a 300 °C 1 s rapid anneal was conducted and studied to determine the change in chemical composition by XPS. After the 300 °C rapid anneal, XPS data showed that the carbon percent for HF-cleaned Si and degreased SiCOH decreased from 14 to 8% and 32 to 28%, respectively. This indicates partial desorption of surface carbon. With less surface carbon, the Si signal from HF-cleaned Si and degreased SiCOH increases.

After 160 supercycles of 30 pulses of $Ti(O^iPr)_4$ followed by 1 pulse of TMA, Si decreases from 82 to 57% and 41 to 16% on HF-cleaned Si and SiO_2, respectively, while degreased SiCOH shows no attenuation of the Si signal. XPS also shows ~10 and ~24% of Al and ~1 and ~3% of Ti on HF-cleaned Si and SiO_2. Based on the equation between the inelastic mean free path and the attenuation length of an electron from the Si substrate (Si signal attenuation), around 0.43 and 0.99 nm TiO_2/Al_2O_3 were calculated to have been deposited on HF-cleaned Si and SiO_2. The TiO_2/Al_2O_3 thicknesses are much less than the thickness estimated from TiO_2 single precursor pulsed CVD with the same $Ti(O^iPr)_4$ total pulse length. The data are consistent, with TMA being the cause for this nucleation prolongation; a simplified model is shown in Figure 2b.

For HfO_2/Al_2O_3, the initial supercycle had 4 pulses of $Hf(O^tBu)_4$ followed by 1 pulse of TMA. XPS of HfO_2/Al_2O_3 on HF-cleaned Si, SiO_2, and degreased SiCOH is shown in Figure 3a. After a total of 35 supercycles (equivalent of 140 Hf pulses), around 2.14, >4 nm, and only 0.1 nm of HfO_2/Al_2O_3 were deposited on HF-cleaned Si, SiO_2, and degreased SiCOH, respectively. Compared with previous HfO_2 300 °C pulsed CVD selectivity study (shown in Figure S6), the same total pulse length of $Hf(O^tBu)_4$ results in a thinner film with TMA as a coreactant. Next, 20 supercycles were deposited consisting of 8 pulses of $Hf(O^tBu)_4$ followed by 1 pulse of TMA to increase the Hf/Al ratio. Around 12, >8 nm, and only 0.29 nm of HfO_2/Al_2O_3 were deposited on HF-cleaned Si, SiO_2 and degreased SiCOH. Selectivity of the deposition increased significantly from 14 (pure HfO_2) to 41 on HF-cleaned Si with TMA codosing. Results indicate that TMA acts as a reactive site eliminator and a selectivity promoter. AFM was also employed to study the film surface roughness, and 0.46 and 0.50 nm RMS roughnesses were measured on Si and SiO_2 in Figure 3b which showed a smooth film surface.

Selectivity Study of TiO_2/Al_2O_3 and HfO_2/Al_2O_3 Nanolaminates. Based on the two novel properties of TMA found in the preliminary study, a detailed selectivity

https://doi.org/10.1021/acsami.1c19810
ACS Appl. Mater. Interfaces 2022, 14, 15716−15727

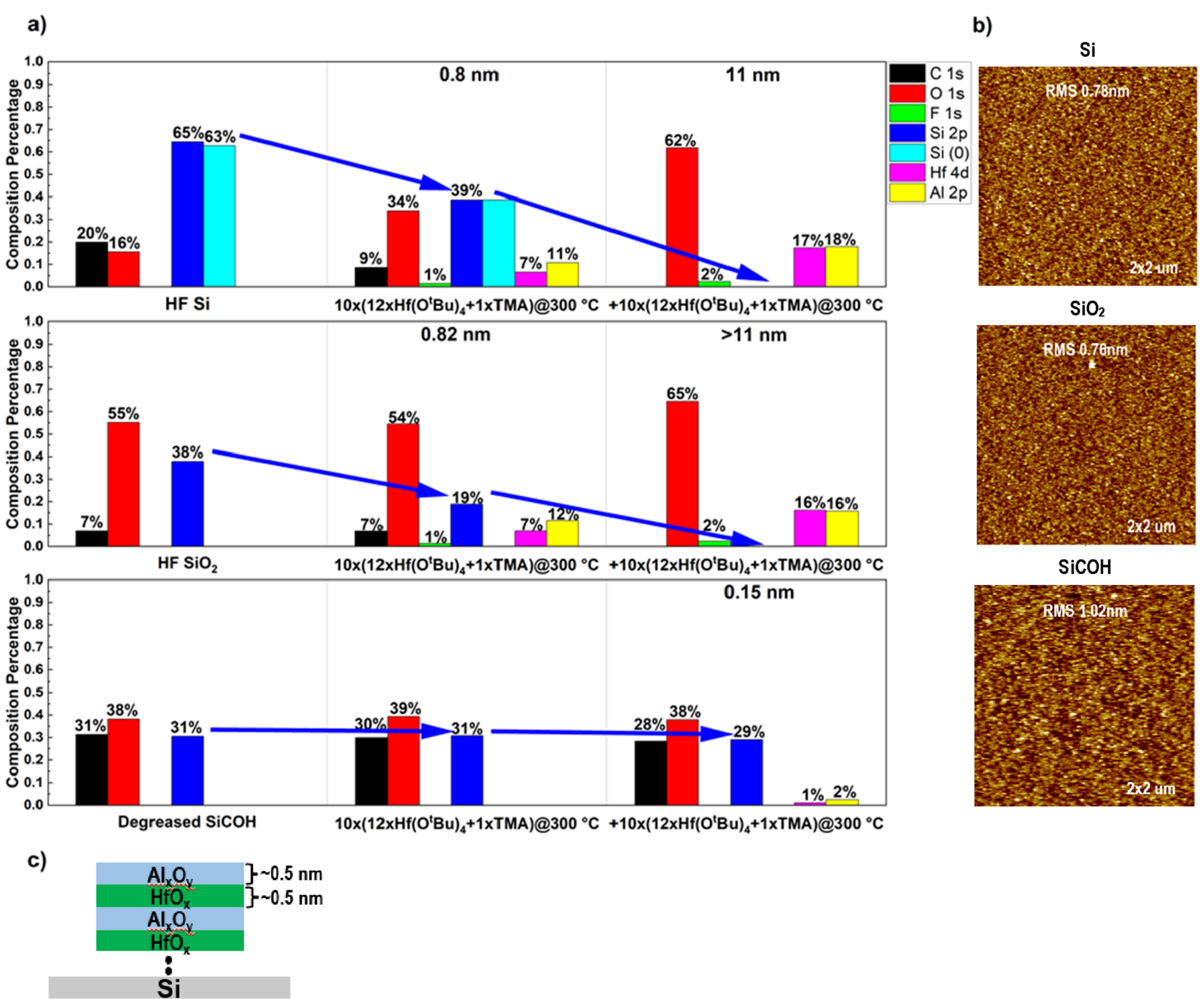

Figure 5. XPS study of selectivity for Hf/AlO_x pulsed CVD. (a) After 300 °C preanneal, XPS of single recipe (12 Hf pulses +1 TMA) $HfAlO_x$ CVD shows that around 11 nm of HfO_2/Al_2O_3 nanolaminate was selectively deposited on Si in preference to SiCOH. Raw data are shown in Figure S10. (b) AFM shows 0.78 and 0.76 nm RMS roughnesses on Si and SiO_2 samples, respectively. (c) Estimated nanolaminate structure composed of 0.5 nm of Al_2O_3 and 0.5 nm of HfO_2.

study of both TiO_2/Al_2O_3 and HfO_2/Al_2O_3 nanolaminates on HF-cleaned Si, SiO_2, and degreased SiCOH was conducted. Considering 30 pulses of $Ti(O^iPr)_4$ per supercycle result in a nucleation delay, a larger number of $Ti(O^iPr)_4$ pulses per supercycle such as 50 and 200 were tested to provide enough reactive sites to initiate the CVD process (shown in Figure S7). With 50 $Ti(O^iPr)_4$ pulses per supercycle, an Al-rich layer was formed, and only around 1 nm of deposition was observed on Si after 45 supercycles (Figure S7).

The number of $Ti(O^iPr)_4$ pulses per supercycle was increased to 200 to check the upper limit of TiO_2 layer thickness before inducing nanocrystallite formation. With an addition of 15 supercycles, a 31 nm TiO_2/Al_2O_3 nanolaminate was deposited on HF-cleaned Si, and only 0.95 nm was deposited on degreased SiCOH (shown in Figure S7a). Around 3 nm/supercycle saturated growth rate on Si can be calculated using ellipsometry thickness measurement 30 nm divided by 10 supercycles. The nanolaminate structure was estimated from the XPS 16:20 Ti/Al ratio, ~1.7 nm of AlO_2, and 1.3 nm of TiO_2 sublayer thickness per supercycle (shown in Figure S7b). A selectivity of 33 was achieved on Si, similar to the single precursor TiO_2 pulsed CVD, but theTiO_2/Al_2O_3 nanolaminate had a completely smooth surface with an RMS roughness of 0.52 nm (see Figure S7). TEM was performed to confirm the nanolaminate structure with an initial Al-rich layer (see Figure S8). From Figure S8, the Al-rich layer was found to be around 0.8 nm, and each superlayer (separated by black dash) is around 2−3 nm. These numbers are consistent with the estimated thickness derived from XPS data.

To validate that 200 pulses $Ti(O^iPr)_4$ followed by 1 pulse of TMA is the ideal nanolaminate CVD process, a fixed 200 pulse $Ti(O^iPr)_4$ per supercycle was carried out on HF-cleaned Si, SiO_2, and degreased SiCOH with only a 300 °C preanneal. After the initial 10 supercycles (incubation period), ~2.9 nm was deposited on HF-cleaned Si with no deposition on SiCOH. With an additional six supercycles, the Si signal from HF-cleaned Si was attenuated to 0% and Si from SiCOH still had 18% (Figure 4a). Film thickness on HF-cleaned Si was measured by ellipsometry to be 22 nm, and only 0.5 nm on SiCOH was deposited. AFM was conducted to confirm a

https://doi.org/10.1021/acsami.1c19810
ACS Appl. Mater. Interfaces 2022, 14, 15716−15727

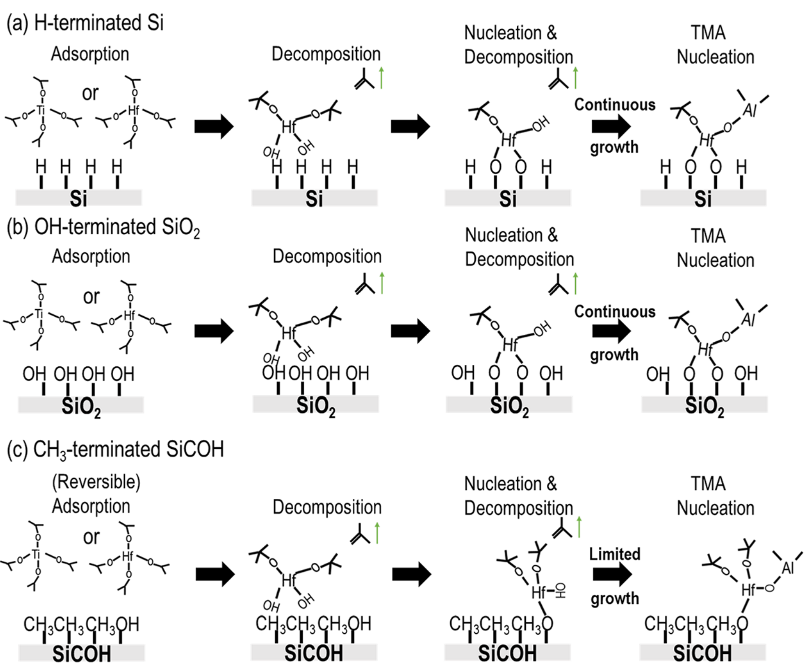

Figure 6. Proposed mechanism of enhancement of HfO_2 and TiO_2 on Si, SiO_2 vs SiCOH with TMA-induced nanolaminate formation. (a,b) On H-terminated Si and OH-terminated SiO_2, precursors can easily adsorb and undergo decomposition due to the high density of reactive sites. (c) CH_3-terminated SiCOH has less adsorption of $Hf(O^tBu)_4$ or $Ti(O^iPr)_4$ on the surface. Defect (OH^-) sites might start nucleation, but the nucleation can be readily suppressed on SiCOH by TMA.

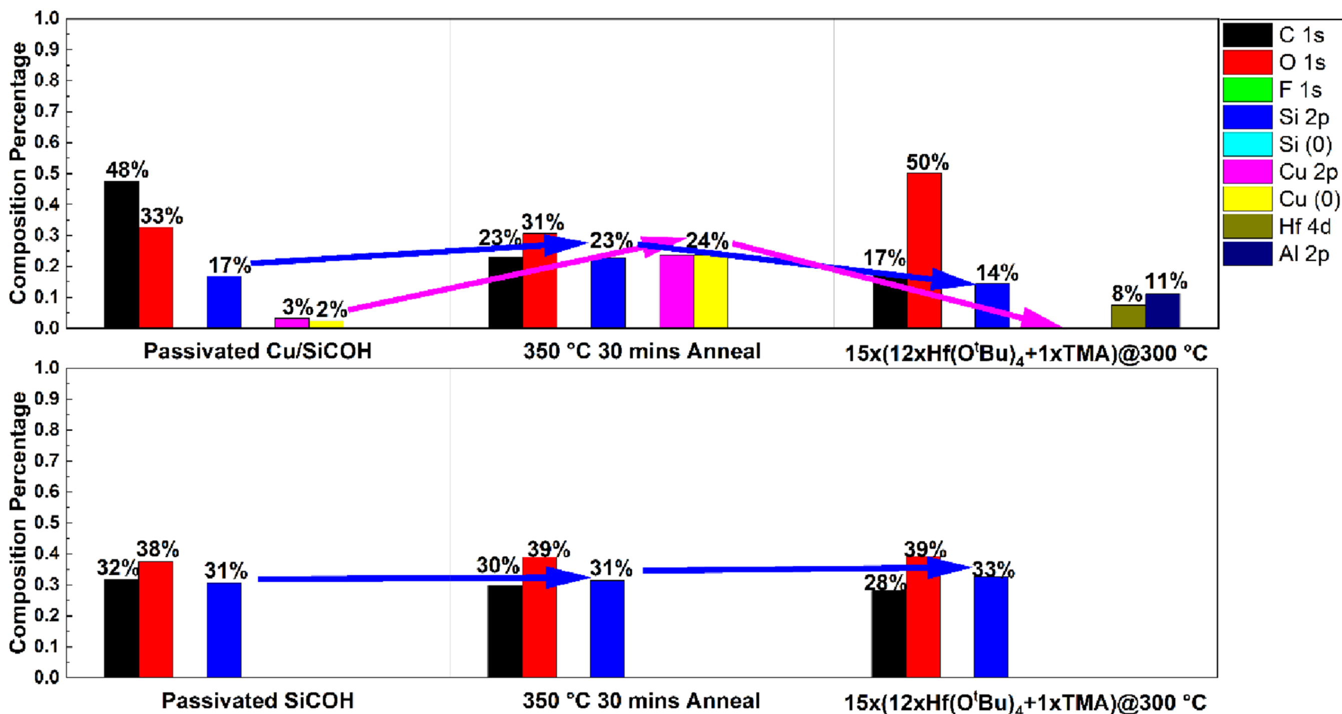

Figure 7. XPS study of nanoselectivity for the HfO_2/Al_2O_3 nanolaminate on a patterned sample. XPS of single recipe (12 Hf pulses + 1 TMA) $HfAlO_x$ CVD shows that at least 5 nm of HfO_2/Al_2O_3 nanolaminate was selectively deposited on the Cu region of the pattern sample while blank SiCOH sample shows no sign of deposition. Raw data is shown in Figure S12.

smooth film surface on both HF-cleaned Si and SiO_2 with RMS roughnesses of 0.38 and 0.4 nm, respectively (Figure 4b). Based on the Ti/Al ratio (16:17), the sublayer thickness of each oxide can be estimated. The nanolaminate structure was composed of 1.5 nm of TiO_2 and 1.6 nm of AlO_2 (Figure 4c). Although 22 nm thickness selective deposition on HF-cleaned Si was less than previous mixed recipe experiment (Figure S7), the calculated selectivity was 44 which showed higher selectivity than single precursor TiO_2 pulsed CVD.

For HfO_2/Al_2O_3 nanolaminates, a sub-monolayer of HfO_2 is equivalent of 10 $Hf(O^tBu)_4$ pulses, and HfO_2 is known to readily form nanocrystallites at 300 °C.[18,38] The single recipe

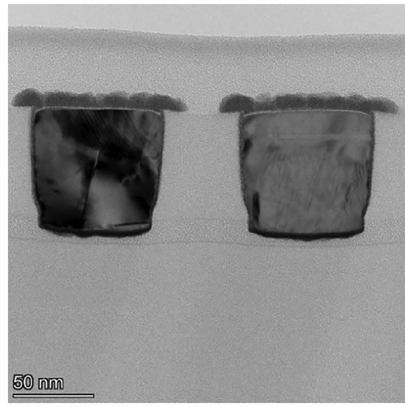

Figure 8. TEM of HfO_2/Al_2O_3 nanolaminate on a patterned sample. TEM image shows that the HfO_2/Al_2O_3 nanolaminate selectively deposited on the Cu region in preference to SiCOH.

for HfO_2/Al_2O_3 nanolaminate CVD supercycle was set as 12 pulses $Hf(O^tBu)_4$ followed by 1 TMA pulse. This allowed HfO_2 sublayers to be thick enough to form a proper nanolaminate structure while staying thin enough to prevent nanocrystallite formation. In Figure 5a, after a total of 20 supercycles, 11 nm of HfO_2/Al_2O_3 was selectively deposited on Si with only 0.15 nm deposition on degreased SiCOH; this corresponds to a selectivity of 73. The selectivity was greatly improved over the single precursor HfO_2 pulsed CVD which has a selectivity of 14. AFM images of both Si and SiO_2 samples showed a smooth HfO_2/Al_2O_3 film (Figure 5b). Based on the Hf/Al (17:18) ratio from the XPS plot, a nanolaminate structure with HfO_2 and AlO_2 alternating subnanometer layers is proposed (Figure 5c).

Mechanism and Nanoselectivity Tests. Based on the selectivity study, a proposed mechanism of selective water-free TiO_2/Al_2O_3 and HfO_2/Al_2O_3 nanolaminates pulsed CVD is shown in Figure 6. In Figure 6a,b, $Hf(O^tBu)_4$ (or $Ti(O^iPr)_4$) adsorbs on the H-terminated Si (H−Si) and OH-terminated SiO_2 ($OH-SiO_2$) surfaces and decomposes into $Hf(O^tBu)_xOH^-_{4-x}$ ($Ti(O^iPr)_xOH^-_{4-}$).[17,18] It is hypothesized that the (OH^-) groups in the intermediate react with weaker bonding H−Si and $OH-SiO_2$ sites inducing chemisorption followed by a continuous growth. Even with TMA being introduced later, there are still enough H−Si or $OH-SiO_2$ reactive sites to nucleate and maintain the growth. Conversely, as shown in Figure 6c, it is posed that the CH_3-terminated SiCOH surface is thermodynamically less favorable for the adsorption of $Hf(O^tBu)_4$. Precursor molecules can be physiosorbed on SiCOH, but most of the precursor will be thermally desorbed before dissociating. Although HfO_2 nucleation might start on (OH^-) defect sites on SiCOH, only limited growth will occur. It is proposed that HfO_2 nucleation will quickly be terminated on SiCOH by TMA since there are very few reactive sites (Si−OH), but TMA has a more modest effect on SiO_2 and Si since they have a much higher density of reactive sites (Si−OH and Si−H, the latter may not be passivated by TMA).

Based on the proposed mechanism, this selective water-free TiO_2/Al_2O_3 and HfO_2/Al_2O_3 nanolaminate pulsed CVD can be applied to any surface with (OH^-) sites (or other reactive sites) in preference to SiCOH. Cu is known to form CuO_x on its surface. Previous result showed that blanket Cu samples have a similar or higher oxide CVD growth rate than SiO_2 (see Figure S11). Selectivity between Cu and SiCOH should be greater than the selectivity study on Si versus SiCOH. Therefore, a Cu/SiCOH patterned sample was employed to test the nanoselectivity of the nanolaminate CVD processes. Due to the damage of SiCOH by the fabrication processes and an extremely long duration (8 months) of air exposure of the patterned sample from the time of fabrication, passivation was needed due to repair the SiCOH.

For each nanoselectivity test, the passivated Cu/SiCOH sample was loaded together with a passivated SiCOH reference

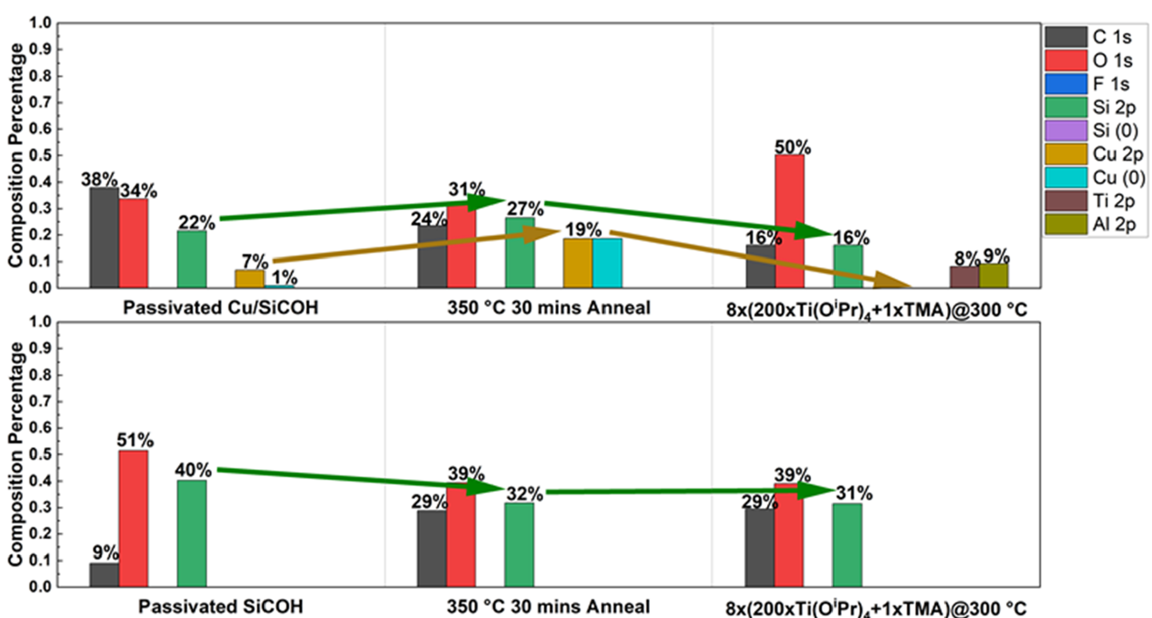

Figure 9. XPS study of nanoselectivity for the TiO_2/Al_2O_3 nanolaminate on a patterned sample. XPS of single recipe (200 Ti pulses + 1 TMA) $TiAlO_x$ CVD shows that at least 5 nm of the TiO_2/Al_2O_3 nanolaminate was selectively deposited on the Cu region of the pattern. Raw data are shown in Figure S14.

https://doi.org/10.1021/acsami.1c19810
ACS Appl. Mater. Interfaces 2022, 14, 15716−15727

Figure 10. TEM and EELS study of TiO_2/Al_2O_3 on the patterned sample. From left to right: (a) bright-field TEM, (b) dark-field TEM, (c) mapping of all elements. (d) Carbon element mapping showed a high intensity layer at the white interface area, copper with carbon overlap mapping proved a thin carbon-rich layer right on top of the copper interface, and a small gap was found between copper and oxygen consistent with the absence of CuO_x formation.

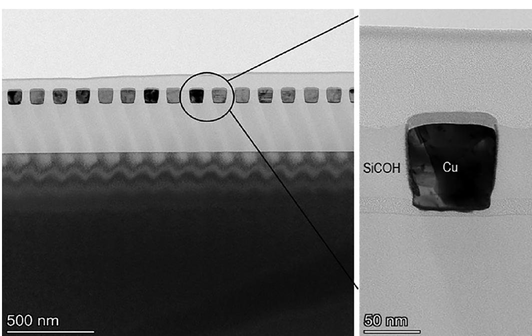

Figure 11. TEM of the TiO_2/Al_2O_3 nanolaminate on a patterned sample. TEM image shows that the TiO_2/Al_2O_3 nanolaminate selectively deposited on the Cu region only with no lateral growth.

sample. TiO_2/Al_2O_3 nanolaminate and HfO_2/Al_2O_3 nanolaminate were independently tested for selectivity.

Cu/SiCOH was processed planarized with standard CMP processing which often involves the use of organics to inhibit Cu oxidation; these organics need to be removed for CVD on the Cu surface. The sample was degreased with acetone, methanol, and water before passivation. Afterward, the patterned sample was rapidly loaded into the chamber. A 30 min 350C UHV anneal was conducted to remove surface organic species. Possible benzotriazole (BTA) residue (a typical Cu oxidation inhibitor) should be mostly removed during the anneal according to the thermal stability studies of BTA.[39,40] Furthermore, XPS shows no CVD induction delay on the Cu surface, consistent with a nearly clean Cu surface being prepared. However, as shown in the cross-sectional TEM EELS study later, there may still be a small amount of carbon on the patterned Cu surface.

HfO_2/Al_2O_3 XPS data plots are shown in Figure 7 for nanoselectivity. The anneal induced the oxygen peak to decrease from 33 to 31% and carbon peak to decrease from 48 to 23% on the patterned sample. With a total of 15 supercycles [12 $Hf(O^tBu)_4$ pulses and 1 TMA pulse], the Cu signal on the patterned sample was decreased to zero which means at least 3−5 nm of HfO_2/Al_2O_3 was deposited on the Cu region. Hf and Al percentages on the pattern sample were 8 and 11%, respectively. The Si signal on the patterned sample also decreased; this is probably due to the X-ray beam interference by nanolaminate deposition. As deposition on Cu region increased, less glancing angle X-ray intensity reached the SiCOH region. The SiCOH reference sample showed no trace

https://doi.org/10.1021/acsami.1c19810
ACS Appl. Mater. Interfaces 2022, 14, 15716−15727

of Al XPS signal which is consistent with little or no deposition on the patterned sample SiCOH region.

After the HfO_2/Al_2O_3 pulsed CVD deposition, TEM was performed on the patterned sample. As shown in Figure 8, around 8 nm of HfO_2/Al_2O_3 was selectively deposited on the Cu region, and no deposition was observed on the SiCOH region. The growth of HfO_2/Al_2O_3 might be following the Volmer−Weber nucleation mode since island structures were observed. The higher reactivity and lower dissociation temperature [compared to $Ti(O^iPr)_4$] of the $Hf(O^tBu)_4$ precursor allows faster nucleation and dissociation. During continuous growth, one $Hf(O^tBu)_4$ can dissociate and provide three additional OH^- reactive sites for sequential dosing which leads to a mushroom-shape isotropic growth and induces formation of the overhang (schematic diagram, please see Figure S13). The observed growth pattern is consistent with Volmer−Weber nucleation, higher dissociation rate, and isotropic growth as well as growth overhang for $Hf(O^tBu)_4$.

Similar XPS results were observed for the TiO_2/Al_2O_3 pulsed CVD deposition on patterned samples as shown in Figure 9. After 30 min of 350 °C anneal, the carbon percentage on the Cu/SiCOH patterned sample dropped from 38 to 24%. The oxygen percent which might come from surface hydrocarbon contamination decreased from 51% to the usual normal 29%. After a total number of eight supercycles [200 $Ti(O^iPr)_4$ pulses with 1 TMA pulse], the Cu signal on the patterned sample disappeared and 8% of Ti and 9% of Al were observed.

As shown in the TEM image in Figure 10, ~10 nm of TiO_2/Al_2O_3 nanolaminate was successfully deposited only onto the Cu substrate, while the SiCOH region remained clean and pristine. The white interfacial layer between Cu and deposition was studied by dark-field TEM and EELS (shown in Figure 10). Dark-field TEM did not show any interfacial layer, but EELS element mapping clearly identified a layer of carbon-rich content on the interface between Cu and the CVD oxide. By overlapping Cu with C and Cu with O, a layer of carbon-rich content was identified on the Cu interface before O signal increase and O mapping shows no signs of CuO_x at the interface. This carbon-rich layer might come from the BTA used in the CMP process or from the oxide CVD process. Selectivity probably could be increased without this carbon-rich layer using a proper preclean method such as H_2 plasma.

The TiO_2/Al_2O_3 nanolaminate appeared to grow only vertically without lateral growth. This may be caused by its lower dissociation rate, higher selectivity, and Cu recess structure resulting from the CMP. From the close-up TEM in Figure 10 and Figure 11, a recess structure was observed on both the top edges of Cu. This recess structure allowed the ALD TaN/Co diffusion barrier to act as a physical vertical wall. Since $Ti(O^iPr)_4$ is less reactive and more selective than $Hf(O^tBu)_4$, it is harder for $Ti(O^iPr)_4$ to nucleate on TaN. With the help of the TaN wall, lower dissociation rate, and anisotropic film growth, no lateral overhang was observed for this thickness of TiO_2/Al_2O_3. This makes the TiO_2/Al_2O_3 nanolaminate a strong candidate for Cu diffusion barrier and etch stop layer.[14−16] Integrated with SAMs that selectively passivated Cu, this nanolaminate can be used as dielectric on dielectric to increase via line critical dimension and improve time-dependent dielectric breakdown.[16] TiO_2/Al_2O_3 nanolaminate may also be a unique spacer material in self-aligned double-patterning method by maintaining the resolution of the feature while reducing the pitch size.

CONCLUSIONS

Inherently selective TiO_2/Al_2O_3 nanolaminates were grown on HF-cleaned Si and SiO_2 in preference to degreased SiCOH by water-free pulsed CVD using $Ti(O^iPr)_4$ and TMA as reactants. The same method was applied to achieve selective HfO_2/Al_2O_3 nanolaminate growth using $Hf(O^tBu)_4$ and TMA as precursors. Employing TMA as the coreactant without water present prolonged the nucleation period on all substrates of both TiO_2/Al_2O_3 and HfO_2/Al_2O_3 nanolaminates, thereby increasing selectivity. For optimal selectivity, TMA needs to be dosed with a controlled pulse length that only increases the nucleation time slightly on HF-cleaned Si and SiO_2 surfaces but induces a long nucleation delay on SiCOH. For the growth stage of the nanolaminate, the number of pulses of the precursor must be set to allow only about 1 nm of growth in the TiO_2 and HfO_2 layers to prevent crystallization and consequently film roughening. For the optimized supercycles, 200 pulses $Ti(O^iPr)_4$ followed by 1 pulse of TMA and 12 pulses $Hf(O^tBu)_4$ with 1 TMA pulse were found to successfully deposit both TiO_2/Al_2O_3 and HfO_2/Al_2O_3 nanolaminates selectively on HF-cleaned Si and SiO_2 in preference to SiCOH. Approximately, 22 nm of TiO_2/Al_2O_3 was deposited on Si, while only 0.5 nm was deposited on SiCOH with a selectivity of 44. Around 11 nm of HfO_2/Al_2O_3 was deposited on Si where nucleation on SiCOH only had 0.15 nm. TEM images of Cu/SiCOH nanoselectivity samples showed that both TiO_2/Al_2O_3 and HfO_2/Al_2O_3 were selectively deposited only on the Cu surface.

ASSOCIATED CONTENT

Supporting Information

The Supporting Information is available free of charge at https://pubs.acs.org/doi/10.1021/acsami.1c19810.

Selectivity comparison between each recipe using the most common selectivity equation; schematic diagram illustrating the custom-built ALD/CVD with in-situ XPS system; XPS study of single precursor TiO2 pulsed CVD; XPS raw spectra of Ti/AlOx CVD; XPS chemical composition study; XPS and AFM studies of nucleation; TEM of mixed recipe; and raw XPS spectra of single recipe (PDF)

AUTHOR INFORMATION

Corresponding Author

Andrew C. Kummel − *Department of Chemistry & Biochemistry, University of California, San Diego, California 92093, United States;* orcid.org/0000-0001-8301-9855; Email: akummel@ucsd.edu

Authors

James Huang − *Materials Science and Engineering, University of California, San Diego, California 92093, United States;* orcid.org/0000-0003-3279-0783

Yunil Cho − *Electrical and Computer Engineering, University of California, San Diego, California 92093, United States;* orcid.org/0000-0002-2680-2015

Zichen Zhang − *Materials Science and Engineering, University of California, San Diego, California 92093, United States;* orcid.org/0000-0001-8028-3271

Antony Jan − *Applied Materials, Incorporated, Santa Clara, California 95054, United States*

Keith T. Wong − *Applied Materials, Incorporated, Santa Clara, California 95054, United States*
Srinivas D. Nemani − *Applied Materials, Incorporated, Santa Clara, California 95054, United States*
Ellie Yieh − *Applied Materials, Incorporated, Santa Clara, California 95054, United States*

Complete contact information is available at:
https://pubs.acs.org/10.1021/acsami.1c19810

Notes

The authors declare no competing financial interest.

ACKNOWLEDGMENTS

Funding support from Applied Materials is gratefully acknowledged. The ellipsometry measurements were facilitated by the San Diego Nanotechnology Infrastructure (SDNI) which is supported by the National Science Foundation (NSF) to Nano3 (grant ECCS-1542148).

REFERENCES

(1) Ito, T.; Okazaki, S. Pushing the Limits of Lithography. *Nature* **2000**, *406*, 1027−1031. Harriott, L. R. *Extended Defects in Germanium*; Springer, 2009; Vol. *89*.
(2) Harriott, L. R. Next Generation Lithography. *Mater. Sci. Semicond. Process.* **1998**, *1*, 93−97.
(3) Mulkens, J.; Hanna, M.; Slachter, B.; Tel, W.; Kubis, M.; Maslow, M.; Spence, C.; Timoshkov, V. Patterning Control Strategies for Minimum Edge Placement Error in Logic Devices. *Metrol. Insp. Process Control Microlithogr. XXXI* **2017**, *10145*, 1014505.
(4) Wu, B.; Kumar, A. Extreme Ultraviolet Lithography and Three Dimensional Integrated Circuit - A Review. *Appl. Phys. Rev.* **2014**, *1*, 011104.
(5) Li, L.; Liu, X.; Pal, S.; Wang, S.; Ober, C. K.; Giannelis, E. P. Extreme Ultraviolet Resist Materials for Sub-7 Nm Patterning. *Chem. Soc. Rev.* **2017**, *46*, 4855−4866.
(6) Buitrago, E.; Meeuwissen, M.; Yildirim, O.; Custers, R.; Hoefnagels, R.; Rispens, G.; Vockenhuber, M.; Mochi, I.; Fallica, R.; Tasdemir, Z.; Ekinci, Y. State-of-the-Art EUV Materials and Processes for the 7nm Node and Beyond. *Extrem. Ultrav. Lithogr. VIII* **2017**, *10143*, 170.
(7) Vincent, B.; Juncker, A.; Clark, W.; Franke, J.-H.; Halder, S.; Lazzarino, F.; Murdoch, G. Self-Aligned Block and Fully Self-Aligned via for IN5 Metal 2 Self-Aligned Quadruple Patterning. *SPIE Adv. Lithogr.* **2018**, *10583*, 221.
(8) Bencher, C.; Chen, Y.; Dai, H.; Montgomery, W.; Huli, L. 22nm Half-Pitch Patterning by CVD Spacer Self Alignment Double Patterning (SADP). *Opt. Microlithogr. XXI* **2008**, *6924*, 69244E.
(9) Dhungana, S.; Nguyen, T. D.; Nordell, B. J.; Caruso, A. N.; Paquette, M. M.; Chollon, G.; Lanford, W. A.; Scharfenberger, K.; Jacob, D.; King, S. W. Boron and High- k Dielectrics: Possible Fourth Etch Stop Colors for Multipattern Optical Lithography Processing. *J. Vac. Sci. Technol., A* **2017**, *35*, 021510.
(10) Majumder, P.; Katamreddy, R.; Takoudis, C. Atomic Layer Deposited Ultrathin HfO2 and Al2O 3 Films as Diffusion Barriers in Copper Interconnects. *Electrochem. Solid-State Lett.* **2007**, *10*, H291.
(11) Chen, H. P.; Shue, W. S.; Cao, M. Fully Self-Aligned Via Integration for Interconnect Scaling Beyond 3nm Node. *2021 IEEE International Electron Devices Meeting (IEDM)*, 2021; pp 486−489.
(12) Doll, G. L.; Mensah, B. A.; Mohseni, H.; Scharf, T. W. Chemical Vapor Deposition and Atomic Layer Deposition of Coatings for Mechanical Applications. *J. Therm. Spray Technol.* **2010**, *19*, 510−516.
(13) Yang, M.; Aarnink, A. A. I.; Schmitz, J.; Kovalgin, A. Y. Inherently Area-Selective Hot-Wire Assisted Atomic Layer Deposition of Tungsten Films. *Thin Solid Films* **2018**, *649*, 17−23.
(14) Choi, J. Y.; Ahles, C. F.; Wong, K. T.; Nemani, S.; Yieh, E.; Kummel, A. C. Highly Selective Atomic Layer Deposition of MoSiOx Using Inherently Substrate-Dependent Processes. *Appl. Surf. Sci.* **2020**, *512*, 144307.
(15) Lemaire, P. C.; King, M.; Parsons, G. N. Understanding Inherent Substrate Selectivity during Atomic Layer Deposition: Effect of Surface Preparation, Hydroxyl Density, and Metal Oxide Composition on Nucleation Mechanisms during Tungsten ALD. *J. Chem. Phys.* **2017**, *146*, 052811.
(16) Mackus, A. J. M.; Merkx, M. J. M.; Kessels, W. M. M. From the Bottom-Up: Toward Area-Selective Atomic Layer Deposition with High Selectivity†. *Chem. Mater.* **2019**, *31*, 2−12.
(17) Cho, Y.; Ahles, C. F.; Choi, J. Y.; Huang, J.; Jan, A.; Wong, K.; Nemani, S.; Yieh, E.; Kummel, A. C. Inherently Selective Water-Free Deposition of Titanium Dioxide on the Nanoscale: Implications for Nanoscale Patterning. *ACS Appl. Nano Mater.* **2022**, *5*, 476−485.
(18) Choi, J. Y.; Ahles, C. F.; Cho, Y.; Anurag, A.; Wong, K. T.; Nemani, S. D.; Yieh, E.; Kummel, A. C. Selective Pulsed Chemical Vapor Deposition of Water-Free HfOx on Si in Preference to SiCOH and Passivated SiO2. *Appl. Surf. Sci.* **2020**, *512*, 145733.
(19) Testoni, G. E.; Chiappim, W.; Pessoa, R. S.; Fraga, M. A.; Miyakawa, W.; Sakane, K. K.; Galvão, N. K. A. M.; Vieira, L.; Maciel, H. S. Influence of the Al2O3 Partial-Monolayer Number on the Crystallization Mechanism of TiO2 in ALD TiO2/Al2O3 Nanolaminates and Its Impact on the Material Properties. *J. Phys. D: Appl. Phys.* **2016**, *49*, 375301.
(20) Ylivaara, O. M. E.; Kilpi, L.; Liu, X.; Sintonen, S.; Ali, S.; Laitinen, M.; Julin, J.; Haimi, E.; Sajavaara, T.; Lipsanen, H.; Hannula, S.-P.; Ronkainen, H.; Puurunen, R. L. Aluminum Oxide/Titanium Dioxide Nanolaminates Grown by Atomic Layer Deposition: Growth and Mechanical Properties. *J. Vac. Sci. Technol., A* **2017**, *35*, 01B105.
(21) Yang, T.; Xuan, Y.; Zemlyanov, D.; Shen, T.; Wu, Y. Q.; Woodall, J. M.; Ye, P. D.; Aguirre-Tostado, F. S.; Milojevic, M.; Mcdonnell, S.; Wallace, R. M. Interface Studies of GaAs Metal-Oxide-Semiconductor Structures Using Atomic-Layer-Deposited Hf O2 Al2 O3 Nanolaminate Gate Dielectric. *Appl. Phys. Lett.* **2007**, *91*, 142122.
(22) Tan, Y. N.; Chim, W. K.; Choi, W. K.; Joo, M. S.; Cho, B. J. Hafnium Aluminum Oxide as Charge Storage and Blocking-Oxide Layers in SONOS-Type Nonvolatile Memory for High-Speed Operation. *IEEE Trans. Electron Devices* **2006**, *53*, 654−662.
(23) Joo, M. S.; Cho, B. J.; Yeo, C. C.; Chan, D. S. H.; Whoang, S. J.; Mathew, S.; Bera, L. K.; Balasubramanian, N.; Kwong, D. L. Formation of Hafnium-Aluminum-Oxide Gate Dielectric Using Single Cocktail Liquid Source in MOCVD Process. *IEEE Trans. Electron Devices* **2003**, *50*, 2088−2094.
(24) Gong, Y.-P.; Li, A. D.; Li, X. F.; Li, H.; Zhai, H. F.; Wu, D. Impact of the Al/Hf Ratio on the Electrical Properties and Band Alignments of Atomic-Layer-Deposited HfO2/Al2O3 on S-Passivated GaAs Substrates. *Semicond. Sci. Technol.* **2010**, *25*, 055012.
(25) Kim, S. K.; Lee, S. W.; Hwang, C. S.; Min, Y.-S.; Won, J. Y.; Jeong, J. Low Temperature (<100°C) Deposition of Aluminum Oxide Thin Films by ALD with O[Sub 3] as Oxidant. *J. Electrochem. Soc.* **2006**, *153*, F69.
(26) Dingemans, G.; Engelhart, P.; Seguin, R.; Mandoc, M. M.; Van De Sanden, M. C. M.; Kessels, W. M. M. Comparison between Aluminum Oxide Surface Passivation Films Deposited with Thermal ALD, Plasma ALD and PECVD. *Conference Record of the IEEE Photovoltaic Specialists Conference*, 2010; pp 3118−3121.
(27) Delabie, A.; Sioncke, S.; Rip, J.; Van Elshocht, S.; Pourtois, G.; Mueller, M.; Beckhoff, B.; Pierloot, K. Reaction Mechanisms for Atomic Layer Deposition of Aluminum Oxide on Semiconductor Substrates. *J. Vac. Sci. Technol., A* **2012**, *30*, 01A127.
(28) Cho, Y.; Huang, J.; Ahles, C. F.; Wong, K.; Nemani, S.; Yieh, E.; Kummel, A. C. Selective Pulsed CVD of HfO2/TiO2 Nanolaminate for Nanoscale Patterning. *IEEE SISC*; San Diego, CA, USA, 2020.
(29) Kwak, I.; Sardashti, K.; Clemons, M. S.; Ueda, S. T.; Fruhberger, B.; Oktyabrsky, S.; Kummel, A. C. HfO2/Al2O3

Nanolaminate on Si 0.7 Ge 0.3 (100) Surface by Thermal Atomic Layer Deposition. *ECS Trans.* **2018**, *86*, 281−289.
(30) Balasubramanian, S.; Mundy, C. J.; Klein, M. L. Trimethylaluminum: A Computer Study of the Condensed Phases and the Gas Dimer. *J. Phys. Chem. B* **1998**, *102*, 10136−10141.
(31) Longo, R. C.; McDonnell, S.; Dick, D.; Wallace, R. M.; Chabal, Y. J.; Owen, J. H. G.; Ballard, J. B.; Randall, J. N.; Cho, K. Selectivity of Metal Oxide Atomic Layer Deposition on Hydrogen Terminated and Oxidized Si(001)-(2×1) Surface. *J. Vac. Sci. Technol., B: Nanotechnol. Microelectron.: Mater., Process., Meas., Phenom.* **2014**, *32*, 03D112.
(32) Grill, A. PECVD Low and Ultralow Dielectric Constant Materials: From Invention and Research to Products. *J. Vac. Sci. Technol., B: Nanotechnol. Microelectron.: Mater., Process., Meas., Phenom.* **2016**, *34*, 020801.
(33) Baklanov, M. R.; Jousseaume, V.; Rakhimova, T. V.; Lopaev, D. V.; Mankelevich, Y. A.; Afanas'Ev, V. V.; Shohet, J. L.; King, S. W.; Ryan, E. T. Impact of VUV Photons on SiO 2 and Organosilicate Low-k Dielectrics: General Behavior, Practical Applications, and Atomic Models. *Appl. Phys. Rev.* **2019**, *6*, 011301.
(34) Krishtab, M.; de Marneffe, J.-F.; Armini, S.; Meersschaut, J.; Bender, H.; Wilson, C.; De Gendt, S. Metal Barrier Induced Damage in Self-Assembly Based Organosilica Low-k Dielectrics and Its Reduction by Organic Template Residues. *Appl. Surf. Sci.* **2019**, *485*, 170−178.
(35) Rezvanov, A. A.; Miakonkikh, A. V.; Seregin, D. S.; Vishnevskiy, A. S.; Vorotilov, K. A.; Rudenko, K. V.; Baklanov, M. R. Effect of Terminal Methyl Group Concentration on Critical Properties and Plasma Resistance of Organosilicate Low-k Dielectrics. *J. Vac. Sci. Technol., A* **2020**, *38*, 033005.
(36) Oszinda, T.; Schaller, M.; Schulz, S. E. Chemical Repair of Plasma Damaged Porous Ultra Low-κ SiOCH Film Using a Vapor Phase Process. *J. Electrochem. Soc.* **2010**, *157*, H1140.
(37) Burrows, V. A.; Chabal, Y. J.; Higashi, G. S.; Raghavachari, K.; Christman, S. B. Infrared spectroscopy of Si(111) surfaces after HF treatment: Hydrogen termination and surface morphology. *Appl. Phys. Lett.* **2013**, *998*, 10−13.
(38) Hausmann, D. M.; Gordon, R. G. Surface Morphology and Crystallinity Control in the Atomic Layer Deposition (ALD) of Hafnium and Zirconium Oxide Thin Films. *J. Cryst. Growth* **2003**, *249*, 251−261.
(39) Grillo, F.; Tee, D. W.; Francis, S. M.; Früchtl, H. A.; Richardson, N. V. Passivation of Copper: Benzotriazole Films on Cu(111). *J. Phys. Chem. C* **2014**, *118*, 8667−8675.
(40) Lim, D. F.; Wei, J.; Leong, K. C.; Tan, C. S. Cu Passivation for Enhanced Low Temperature (≤300 °C) Bonding in 3D Integration. *Microelectron. Eng.* **2013**, *106*, 144−148.

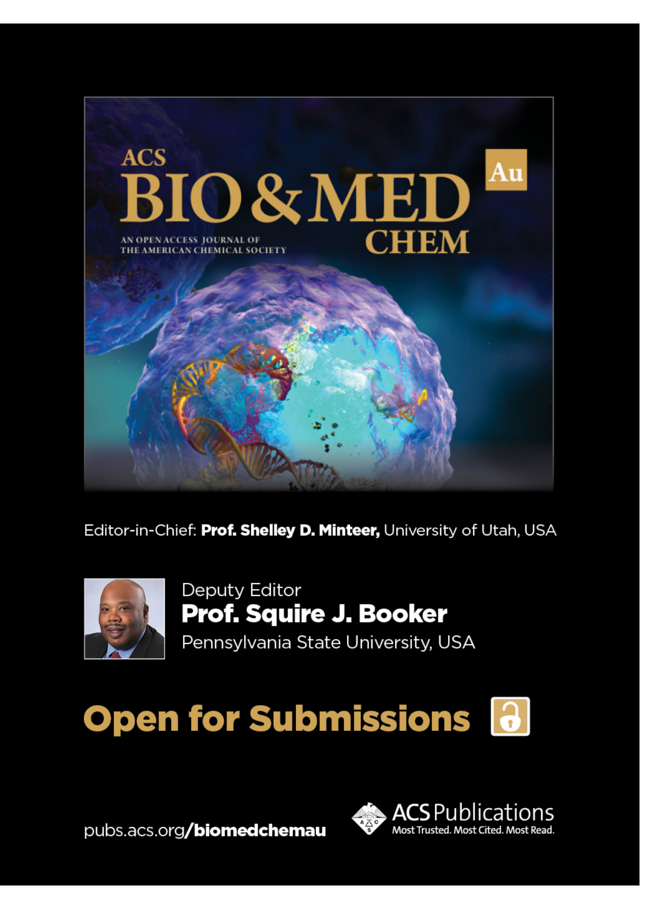

https://doi.org/10.1021/acsami.1c19810
ACS Appl. Mater. Interfaces 2022, 14, 15716−15727